PERIODICO di MINERALOGIA
established in 1930

DIPARTIMENTO
DI SCIENZE DELLA TERRA
SAPIENZA
UNIVERSITÀ DI ROMA

An International Journal of
Mineralogy, Crystallography, Geochemistry,
Ore Deposits, Petrology, Volcanology
and applied topics on Environment, Archaeometry and Cultural Heritage

Potentially toxic elements distribution in the serpentinized and deformed ultramafic rocks from the Voltri Massif (NW, Italy)

Silvia Fornasaro [1], Paola Comodi [2], Laura Crispini [1],
Cristina Malatesta [1], Azzurra Zucchini [2], Pietro Marescotti [1,*]

[1] DISTAV, University of Genova, C.so Europa 26, 16132 Genova, Italy
[2] Department of Physics and Geology, University of Perugia, P.zza Università, 06123 Perugia, Italy

ARTICLE INFO

Submitted: April 2019
Accepted: June 2019
Available on line: July 2019

* Corresponding author:
pietro.marescotti@unige.it

DOI: 10.2451/2019PM874

How to cite this article:
Fornasaro S. et al. (2019)
Period. Mineral. 88, 259-276

ABSTRACT

The aim of the work is to assess the role of local-scale lithological, textural, and structural factors in the distribution of potentially toxic elements (PTEs) in different ultramafic rocks from the high-pressure ophiolitic Voltri Massif (Central Liguria, NW Italy). The results evidenced that Cr (up to 4183 ppm), Ni (up to 3900 ppm), and Co (up to 334 ppm) are invariably the PTEs with the highest concentrations; in addition, V, Cu, and Zn are systematically found in non-negligible amounts. Spinel-group minerals (chromium spinel, ferrian chromite, chromium magnetite, and magnetite) are by far the main potential source of the PTEs. Nevertheless, several PTEs are also present within serpentines, olivines, pyroxenes, chlorites, as well as within accessory phases (e.g., ilmenite and Ni-sulphides) and within authigenic minerals formed in the early stages of rock weathering (cryptocrystalline to amorphous Fe-oxides and -oxyhydroxides).
The result obtained allowed to evidence that the main factors controlling the PTEs distribution within the rocks resulted to be the serpentinization degree and the deformation style and intensity which, in turn, strictly control the mineral assemblages and the mineral chemistry.

Keywords: geogenic source; serpentinization; geochemical background; potential toxic elements; Voltri Massif; Liguria.

INTRODUCTION

High concentrations of potentially toxic elements (PTEs) in surface and near-surface environment may be attributed both to anthropogenic sources (including industrial, agricultural, and mining activities) and to geogenic sources (e.g., natural weathering of rocks and pedogenesis).

Among the geogenic sources, ultramafic rocks (e.g., dunite, peridotite, pyroxenite, and serpentinite) are the most critical from the environmental point of view because they are invariably characterized by high amounts of Cr (up to 15300 ppm; Stueber and Goles, 1967), Ni (up to 7733 ppm; Savov et al., 2007), and Co (up to 950 ppm; Garnier et al., 2009).

Despite a general similarity in the whole rock chemical composition, the concentration and distribution of PTEs in ultramafic rocks is highly variable. In general, PTEs content can range up to two orders of magnitude, mainly because of heterogeneities in mineralogy and mineral chemistry, texture, and structural properties of the ultramafic rocks (Kierczak et al., 2016; Echevarria, 2018). All these factors are strictly related to the different geological settings as well as to their metamorphic and geodynamic evolutions (Deschamps et al., 2013).

In general, the mineralogical composition of the primary ultramafic rocks is dominated by the presence of Mg- and Fe-rich silicate minerals (e.g., olivines and pyroxenes) and spinel-group minerals (e.g., chromite and

magnetite). Serpentinization causes the formation of a large variety of metasomatic and metamorphic minerals such as serpentines (lizardite, chrysotile, and antigorite), chlorites and clay minerals, amphiboles (e.g., tremolite and actinolite), talc, brucite, iron oxides, and carbonates, possibly incorporating variable concentrations of PTEs into their crystal structures.

The weathering of ultramafic rocks produces soils containing high concentrations of Cr, Ni, and Co (Oze et al., 2004 a,b; Alexander, 2007) that, in suitable pedogenic conditions, can reach even economic significance (e.g., Ni-laterites; Butt and Cluzel, 2013). Most significantly, the high concentrations of PTEs in soils can have a potentially harmful impact on ecosystems and human health if released into waters.

Mineral stability and therefore element mobility and bioavailability are strictly related to the mineralogical assemblage. As an example, Ni is generally more mobile than Cr because the latter is bounded in more weathering-resistant minerals (i.e., chromite and Cr-bearing magnetites; e.g., Kierczak et al., 2007; Quantin et al., 2008; Cheng et al., 2011).

Considering the strong environmental implications deriving from the occurrence of ultramafic rocks, the detailed knowledge of the variation in mineralogy and crystal chemistry of these rocks can thus help to understand the distribution of PTEs and their fate during weathering processes, playing an important role also in environmental management (Kumarathilaka et al., 2014; Tashakor et al., 2014).

The aim of this study is to assess the role of meso- and micro-scale lithological, mineralogical, textural, and structural variations in controlling concentration and distribution of PTEs (V, Cr, Co, Ni, Cu, and Zn) in serpentinized ultramafic rocks. In order to achieve this target, we studied high pressure-low temperature (HP-LT) ultramafites of the Voltri Massif (Central Liguria, Italy), which is one of the widest metaophiolite outcrops in the Western Alps.

GEOLOGICAL SETTING

The study area is located in the NW area of the Voltri Massif (VM), a wide metaophiolitic body (about 800 km^2) at the southernmost termination of the Western Alps (Ligurian Alps, NW Italy; Figure 1).

The VM represents a remnant of the Jurassic Ligurian Tethys and is composed by tectono-metamorphic units accreted during the Alpine orogenesis (Capponi and Crispini, 2008 and references therein). These units consist mainly of mafic to ultramafic rocks derived from different paleogeographic domains, including subcontinental mantle, oceanic lithosphere with sedimentary covers, and subordinate continental crust (Capponi et al., 2016). The units of the VM show a polyphase tectono-metamorphic evolution with blueschist- to eclogite facies peak metamorphism and variable retrogressive overprints down to greenschist facies (e.g., Messiga et al., 1983; Malatesta et al., 2012 and reference therein; Capponi et al., 2016; Scarsi et al., 2018).

The study area comprises serpentinized peridotites and antigorite serpentinites of the VM (Figure 1). In the VM peridotites occur as km-scale bodies and consist mainly of spinel- and plagioclase-bearing lherzolite, with minor harzburgite, dunite lenses and pyroxenite bands. They are affected by a various degree of serpentinization that develops mainly along networks of anastomosing shear zones that separate domains of low-deformed to undeformed peridotites (Scambelluri et al., 1991).

Antigorite serpentinites are composed of antigorite-bearing massive serpentinites and antigorite-bearing serpentine schists, sometimes with textural relics of the mantle peridotites. They represent the most abundant lithotype of the VM, cropping out over a total area of more than 200 km^2. Gradual transitions from massive and essentially undeformed to strongly foliated serpentinite (serpentine schist) occur over the entire study area. Serpentine schists are commonly characterized by a pervasive composite schistosity, with multiple folding phases and shear bands (Scambelluri et al., 1991; Malatesta et al., 2012; Federico et al., 2015; Capponi et al., 2016 and reference therein).

Finally, chlorite/talc-schist or tremolite-chlorite schists (i.e., "hybrid" rocks, Spandler et al., 2008), including chlorite, talc, tremolite, actinolite, albite, titanite and magnetite, are common as intercalations or reaction rims at the contact among serpentinites and other lithotypes (e.g., metasediments and ecolgites Hoogerduijn Strating, 1991; Federico et al., 2007; Malatesta et al., 2012).

MATERIAL AND METHODS

A preliminary detailed geo-structural survey was performed in eight sites (Table 1) of the VM with good exposures of ultramafic rocks (e.g., roadcut, abandoned quarries, stream banks), that were representative of significant structural and textural variations.

The studied rocks were grouped into three main groups (Table 1): i) partially serpentinized peridotite (PSP) with a serpentinization overprint that ranges between 50 to 90 %; ii) massive serpentinites (MS) with a prevailing undeformed massive texture, with a serpentinization degree that ranges between 90% to 100%; iii) foliated serpentinites (FS) with a serpentinization degree close to 100%.

Forty-five rock samples have been selected according to i) the different degree of serpentinization (based on the modal abundance of serpentine minerals), ii) textures

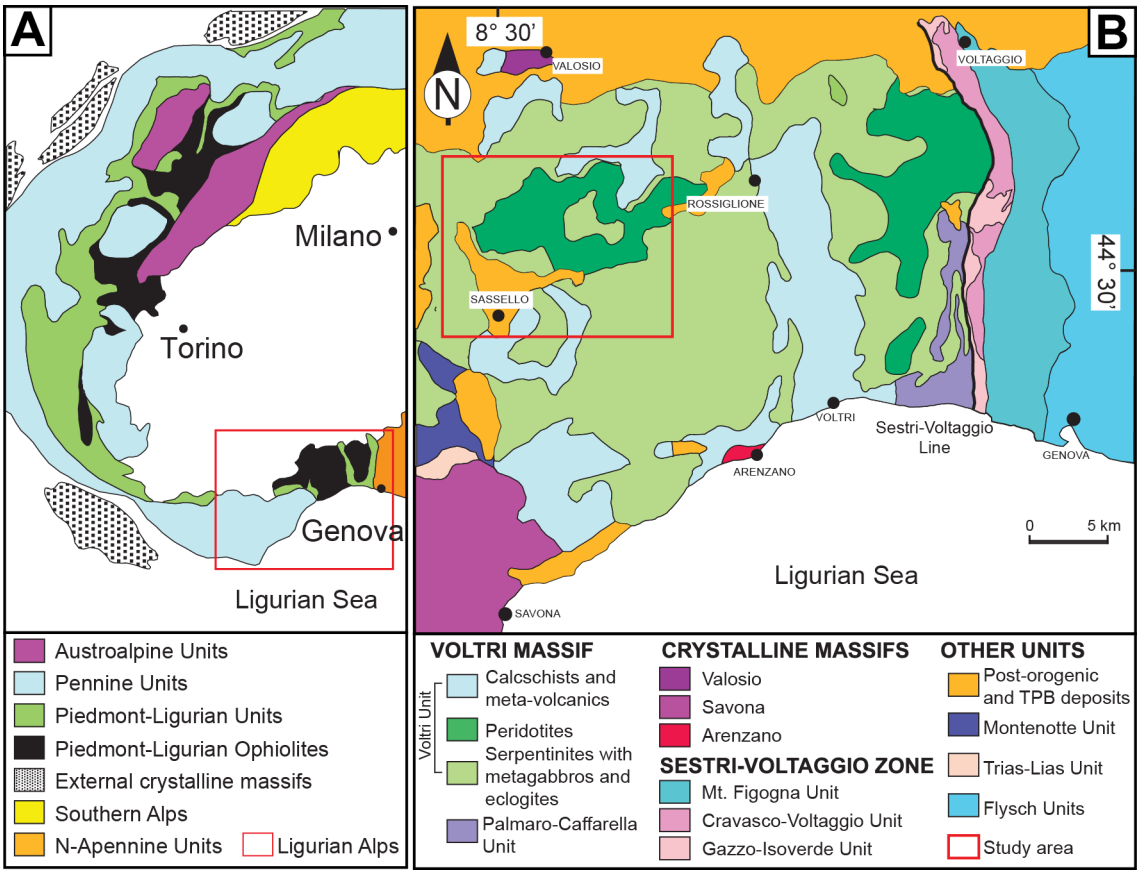

Figure 1. A) Sketch map of the Western Alps; B) Geological map of the Voltri Massif and adjoining Units. Modified after Capponi and Crispini (2002).

Table 1. Geographical and lithological information of the studied sites (PSP=partially serpentinized peridotite; MS=massive serpentinite; FS=foliated serpentinite).

Site	Coordinates (WGS84)	Outcrop type	Altitude (m a.s.l.)	Slope exposition	Lithotypes
Bric Gippone	44°29'12.0"N, 8°30'51.5"E	Road cut	585	S	MS/FS
Badia Tiglieto	44°31'31.6"N, 8°36'06.7"E	Abandoned quarry	380	S	FS
Case Lavrin	44°29'46.9"N, 8°35'10.4"E	Abandoned quarry	668	ESE	FS
Diga Antenna	44°28'56.1"N, 8°35'45.4"E	Road cut	580	SW	FS
Strada Giusvalla	44°26'53.1"N, 8°25'32.4"E	Road cut	433	SE	MS
Rocca Grin	44°30'10.2"N, 8°32'32.5"E	Abandoned quarry	626	SW	PSP
Strada Ferriera	44°26'02.3"N, 8°25'27.7"E	Road cut	576	SSE	MS
Torrente Orba	44°31'02.7"N, 8°37'22.8"E	Stream banks-Abandoned quarry	418	W	FS

(e.g., massive vs foliated serpentinites), and iii) structural features (e.g., occurrence and distribution of veins and/or fractures).

The rock samples have been analyzed using a multiscale and multi-analytical approach including: i) mineralogical and petrographic description and microstructural analysis by means of polarized-light optical microscopy and scanning electron microscopy (SEM-EDS); ii) qualitative and quantitative mineralogical analyses by means of X-ray powder diffraction (XRPD); iii) chemical analyses of minerals by means of electron microprobe analyzer (EMPA-WDS) and laser ablation-inductively coupled plasma-mass spectrometry (LA-ICP-MS); iv) bulk rock chemical analyses by means of energy dispersive X-ray fluorescence (EDXRF) and inductively coupled plasma-atomic emission spectroscopy (ICP-AES).

SEM-EDS analyses have been performed on selected representative carbon-coated thin sections of studied rock samples at the Department for Earth, Environmental and Life Sciences (DISTAV) of the University of Genova (Italy), using a SEM Vega3 - TESCAN type LMU system equipped with an EDS EDAX APOLLO XSDD with DPP3 analyzer. Analyses were performed at the following conditions: 20 kV accelerating voltage, 1.2 nA beam current, 10-40 mm beam diameter, 15 mm working distance. Counting times were set at 60 s to prevent damage to the coated surface. Calibration for chemical analyses was accomplished with a set of synthetic and natural standards.

XRPD analyses were performed on selected samples at the Department of Physics and Geology, University of Perugia (Italy) and were carried out using a Philips PW1830 diffractometer equipped with a Cu-anode (CuKα radiation; range 5-80° 2θ; step size 0.02° 2θ). Metallic silicon (10 wt%) was added as standard for amorphous phases quantification. Rietveld refinements were performed with General Structure Analysis Software (GSAS; Larson and Von Dreele, 2004), following the procedure described in Frondini et al. (2014). Data refinements were carried out starting from atomic coordinates and cell parameters of antigorite (Capitani and Mellini, 2006), chrysotile (Falini et al., 2004), augite (Gualtieri, 2000), enstatite (Bystrom, 1943), clinochlore (Zanazzi et al., 2006), forsterite (Bostrom, 1987), tremolite (Hawthorne and Grundy, 1976), albite (Gualtieri, 2000), magnetite (Wright et al., 2000).

The most representative samples (eleven carbon-coated metallographic sections) were analyzed by the EMPA-WDS JEOL 8200 Super Probe at the Department of Earth Sciences "Ardito Desio", University of Milano (Italy). The working conditions were set at 15 kV accelerating voltage and 4.9 nA beam current. Calibration for chemical analysis was accomplished by using the following standards: olivine (Mg), omphacite (Na), Cr_2O_3 (Cr), rhodonite (Mn and Zn), k-feldspar (K), anorthite (Al and Ca), wollastonite (Si), pure V, fayalite (Fe), ilmenite (Ti), CoO (Co), galena (S), niccolite (Ni).

Trace and ultra-trace elements of selected minerals (e.g., olivines, pyroxenes, serpentines, and spinel-group minerals) were determined with detection limits below ppm units by laser ablation-inductively coupled plasma-mass spectrometry (LA-ICP-MS) at the Department of Physics and Geology, University of Perugia (Italy); details on the working conditions, instrumentation, precision, and accuracy are reported in Petrelli et al. (2016).

Bulk chemical analyses were assessed by means of X-MET7500 (Oxford Instruments) EDXRF spectrometer (GeoSpectra s.r.l. - Spin-Off company of the University of Genova) and by ICP-AES at the Regional Agency for Environmental Protection of Liguria (ARPAL, Genova, Italy), using a Perkin Elmer - Optima 2100 DV spectrometer, on 3.5 g sample powder after total digestion of the material by melting with aqua regia (1 cc HNO_3+2 cc HCl).

RESULTS

Mineralogy, petrography and microstructures

Partially serpentinized peridotites (PSP)

PSP form metric to pluri-metric bodies rimmed by decametric- to metric-thick serpentinitic shear zones; they are medium (1-5 mm) to coarse- (5-10 mm) grained rocks displaying a granular to porphyroblastic texture with pyroxene crystals (up to 5 mm) that are locally oriented allowing to identify a weakly preserved primary mantle foliation.

PSP commonly show pseudomorphic textures (i.e., mesh textures and bastites) with relics of forsteritic olivine (Fo89), clinopyroxenes (augite and diopside), enstatite (sometimes partially replaced by amphiboles), and spinel-group minerals (mainly Cr-spinel; Figure 2A).

Antigorite and magnetite are the main minerals within mesh textures and bastites, with subordinate chrysotile and chlorite within mesh rims and along grain boundaries. Locally, mm-thick mylonitic shear zones cut the pseudomorphic textures isolating sigmoidal-shape domains where the mesh textures evolve to hourglass, ribbon and/or interpenetrating textures from the centre toward the rims. The outer mylonitic shear zones are exclusively composed by synkinematic antigorite, intimately intergrown with chlorite, and fine-grained magnetite and Cr-magnetite. Along shear-zone antigorite±chrysotile bastites are commonly deformed and pervasively kinked.

PSP are generally crosscut by several veins, which can be grouped as follow on the basis of spatial relationships and filling (Figures 3A-F): 1) syntaxial submillimetric veins (up to ~200 μm in width) mainly occurring in the domains

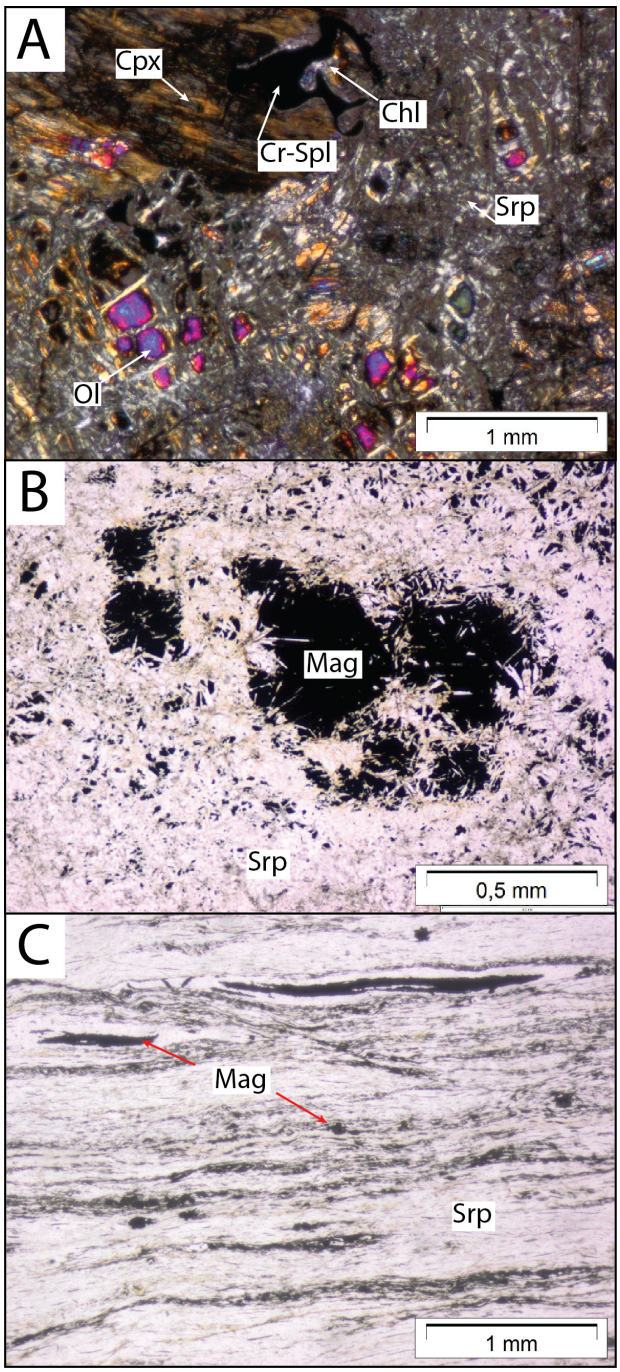

Figure 2. Photomicrographs of the studied ultramafic rocks: A) mesh texture with olivine relics and bastitic pyroxenes (PSP; crossed-polarized light - XPL); B) magnetite and serpentine minerals aggregates within interpenetrating texture (MS; plane-polarized light - PPL); C) fine-grained magnetite-rich layers within an antigorite-rich domain characterized by a pervasive schistosity (FS; PPL). Mineral abbreviations after Whitney and Evans (2010).

preserving pseudomorphic textures; these veins are filled with chrysotile cross-fibers, growing symmetrically from the vein rims, and subidiomorphic magnetite crystals along the median line (Figure 3A); 2) millimetric stretched veins (up to ~2 mm in width) crosscutting the foliation and filled with chrysotile cross-fibers±talc±brucite (Figure 3B); 3) shear veins (up to ~100 μm in width) parallel to foliation and connected with extensional veins at high angles; they are mainly filled with deformed slip-fibers of chrysotile with minor talc and magnetite (Figure 3C); 4) sigmoidal veins and en-échelon veins (5-70 μm in width) with a random spatial distribution, filled with fibrous chlorite and chrysotile (Figure 3D); 5) composite veins (up to ~2 mm in width) crosscutting the foliation and the other set of veins (1-4); they are mainly filled with fibrous talc associated with minor chrysotile and magnetite (Figure 3E); 6) micrometric magnetite veinlets (<50 μm) forming an irregular network and crosscutting all the other vein sets; magnetite is commonly oxidized, with oxidation patterns along the vein rims and oxidation halos in the adjoining selvages (Figure 3F).

The overall mineralogical composition of PSP is represented by antigorite (26-49 wt%; Figure 4A) chrysotile (8-27 wt%, which the higher concentration in the highly fractured samples), clinochlore (7-26 wt%), augite, (16-32 wt%), enstatite (5-7 wt%), and spinel-group minerals (mainly magnetite and subordinate Cr-spinels; up to 5 wt%). Forsteritic olivine and actinolite-tremolite amphibole locally occur and generally vary from 1 to 3 wt%. Cryptocrystalline authigenic Fe-oxide and oxyhydroxides form oxidation halos around fractures, mylonitic zones, and grain boundaries (mostly around olivine and magnetite). These authigenic minerals correspond mostly to the amorphous phases and/or to low crystalline minerals quantified by Rietveld refinement (1-12 wt%; Figure 4A).

The most common accessory minerals are talc and brucite, occurring associated with chrysotile within veins (Figure 3E).

Massive serpentinites (MS)

MS occur as metric lenses wrapped by decimetric- to metric-thick cataclastic or mylonitic areas; they are medium- (1-5 mm) to fine-grained (<1 mm) serpentinite and display a massive texture with rare spinel-group minerals porphyroclasts (up to 5 mm).

Antigorite-bearing interpenetrating textures with scattered magnetite and/or Cr-magnetite porphyroblasts are predominant and minor pseudomorphic textures (such as mesh, hourglass, ribbon, and bastitic textures) are locally preserved (Figure 2B). In these textures, antigorite shows lamellar, acicular, and less frequently pseudo-fibrous morphology. Magnetite occurs also in trails of

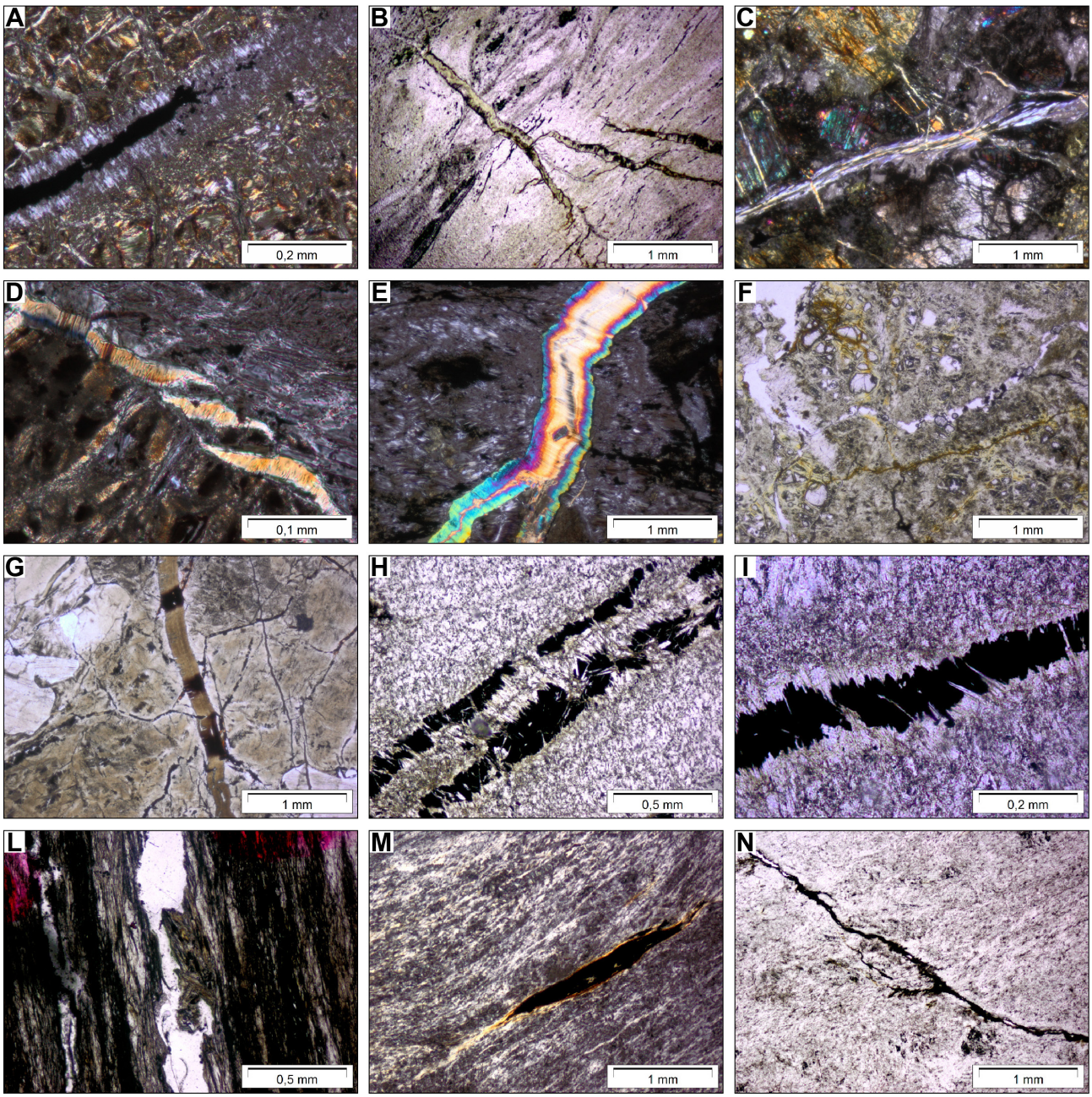

Figure 3. Photomicrographs of the vein systems in the studied rocks. Vein systems in PSP: A) syntaxial veins filled by chrysotile cross-fibers and magnetite (XPL); B) stretched veins filled by chrysotile cross-fibers (PPL); C) shear veins filled by chrysolite slip-fibers (XPL); D) sigmoidal veins filled by chrysotile and chlorite (XPL); E) composite veins filled by talc and chrysotile (XPL); F) oxidized magnetite veinlets (PPL). Vein system in MS: G) stretched veins filled by chrysotile cross-fibers (PPL); H) antitaxial veins filled by magnetite and chrysotile cross-fibers (PPL); I) syntaxial veins filled by magnetite and chrysotile cross-fibers (PPL). Vein systems in FS: L) shear veins filled by chrysotile slip-fibers (PPL); M) sigmoidal veins filled by magnetite (XPL); N) magnetite veinlet (PPL).

micrometric crystals or in pseudo-rounded aggregates associated with antigorite. Fine-grained magnetite forms coronas around bastites or occurs along the mineralogical cleavage of former pyroxene. Magnetite and chrysotile are also the more common minerals within veins.

MS are generally crosscut by several veins, which can be grouped as follow on the basis of spatial relationships and filling (Figures 3, G-I): 1) stretched millimetric

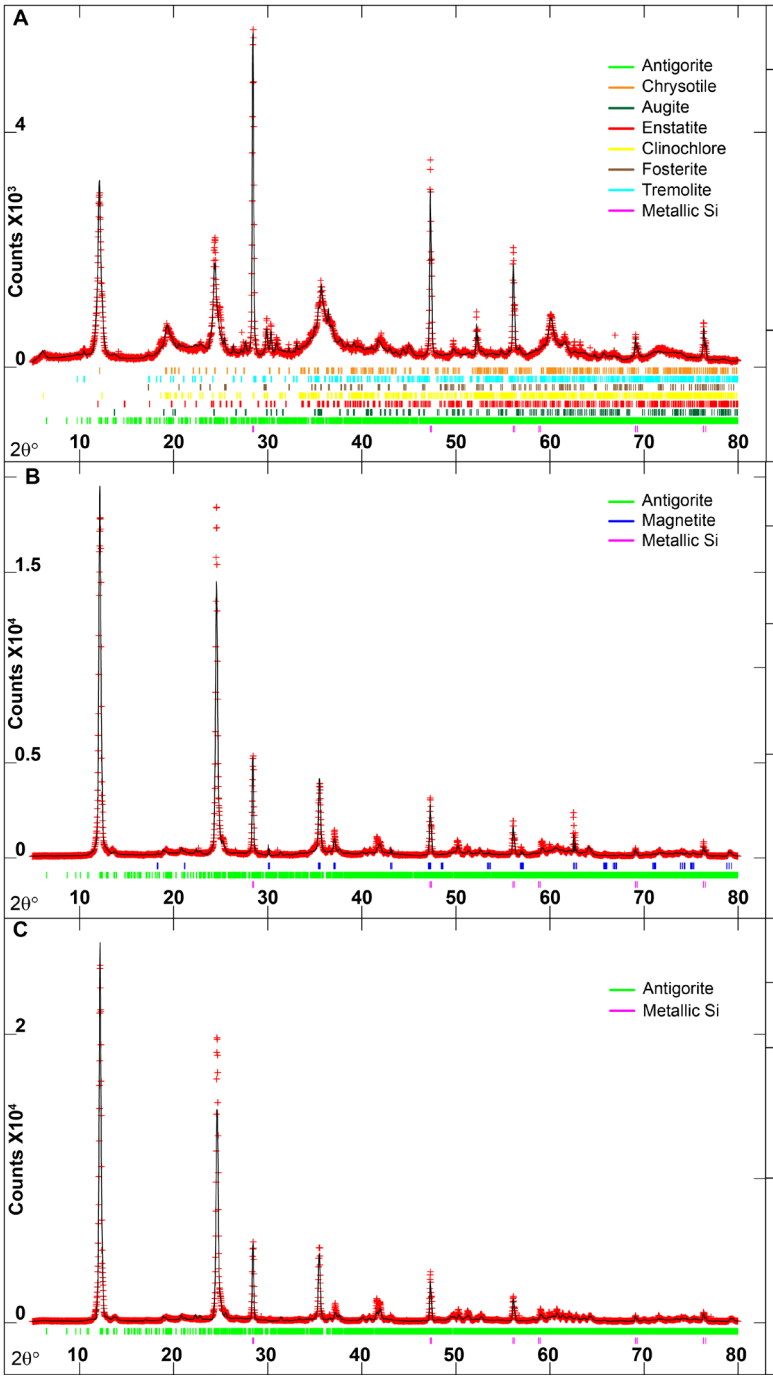

Sample	RG_R2B
Rock	PSP
Antigorite	26.14
Chrysotile	8.45
Augite	17.11
Enstatite	5.26
Clinochlore	25.69
Forsterite	2.75
Tremolite	2.75
Amorphous	11.54
N° reflections	6784
N° observations	3750
Rp	0.0959
Rwp	0.1233

Sample	BG_R3
Rock	MS
Antigorite	85.72
Magnetite	2.43
Amorphous	11.85
N° reflections	3849
N° observations	3750
Rp	0.1513
Rwp	0.1925

Sample	BG_R1
Rock	FS
Antigorite	96.7
Amorphous	3.3
N° reflections	3714
N° observations	3750
Rp	0.1638
Rwp	0.2104

Figure 4. Representative XRPD pattern and quantitative phases analysis calculated from Rietveld refinement of A) PSP B) MS, and C) FS samples. Experimental data and calculated profiles are shown as red crosses and black solid lines, respectively. The coloured thick lines at the bottom of the spectra represent the theoretical Bragg positions of recognized mineral phases. The amounts of solid phases are in wt%.

veins (up to ~1 mm in width) filled with chrysotile cross-fibers±talc±magnetite sometimes replaced by secondary Fe-oxyhydroxides (Figure 3G); 2) antitaxial submillimetric veins (up to ~500 µm in width) filled with elongated magnetite crystals arranged symmetrically at the vein rims and chrysotile cross-fibers along the median line (Figure 3H); 3) syntaxial submillimetric veins (up to ~200 µm in width) filled with chrysotile cross-fibers growing symmetrically from the vein rims and subidiomorphic magnetite crystals along the median

line (Figure 3I); 4) micrometric magnetite veinlets (<50 μm) forming an irregular network and crosscutting all the other vein sets; magnetite is commonly oxidized, with oxidation patterns along the vein rims and oxidation halos in the adjoining selvages.

The main mineralogical phase of MS is antigorite (ranging from 71 to 98 wt%), with subordinate magnetite (up to 10 wt%), chrysotile (<1 wt%), talc (<1 wt%), and chlorite (<1 wt%) (Figure 4B). Authigenic Fe-oxide and oxyhydroxides form commonly oxidation halos around fractures and grain boundaries (mostly around magnetite); they are generally cryptocrystalline and correspond mostly to the amorphous phases and/or to low crystalline minerals quantified by Rietveld refinement (2-26 wt%; Figure 4B).

Foliated serpentinites (FS)

FS occur as decimetric- to metric-thick layers that wrap massive serpentinite domains, as a result of a variable strain partitioning in the most deformed zones. FS are fine- (<1mm) to medium-grained (1-5 mm) rocks with rare scattered sub-idiomorphic magnetite porphyroclasts (3-5 mm; Figure 2C). FS generally show a pervasive foliation that is locally deformed by open folds.

This pervasive foliation, that is the main structural feature of FS, is defined by syn-kinematic lamellar or prismatic antigorite, acicular chlorite, microcrystalline magnetite, and minor apatite±zircon. Rootless hinges of intrafoliar folds, with axial surfaces parallel to the main foliation, are preserved and define a composite fabric. The composite fabric is deformed by a later crenulation cleavage with an axial surface at a high angle with respect to the foliation. Locally, sigmoidal boudins along the foliation preserve domains with antigorite-rich pseudomorphic (ribbon and bastite textures) and non-pseudomorphic textures. Syn-kinematic mm-sized magnetite often borders sigmoidal boudins together with ilmenite. Magnetite occurs also as mm-sized porphyroclasts along the foliation, showing brittle deformation patterns (i.e., bookshelf structures). Clinopyroxenes (mostly diopside) occur locally as relics along the foliation.

FS are generally crosscut by several vein systems, which can be grouped as follow on the basis of spatial relationships and filling (Figures 3, L-N): 1) shear veins (up to ~100 μm in width) parallel to the foliation and mainly filled with deformed slip-fibers of chrysotile with minor talc and magnetite (Figure 3L); 2) sigmoidal veins (100-300 μm in width) arranged parallel to the foliation and filled with microcrystalline magnetite mostly oxidized along the vein rims from which oxidation halos spread toward the adjoining selvages (Figure 3M); 3) micrometric magnetite veinlets (<50 μm) forming an irregular network and crosscutting all the other vein sets (Figure 3N).

Antigorite represents approximately the 92% of the overall mineralogical composition (ranging from 94 to 91 wt%), with subordinated magnetite (up to 5 wt%), chrysotile (<1 wt%), and chlorite (<1 wt%) (Figure 4C). Cryptocrystalline authigenic Fe-oxide and oxyhydroxides form oxidation halos around foliation, fractures, mylonitic zones, and grain boundaries. They correspond mostly to the amorphous phases and/or to low crystalline minerals quantified by Rietveld refinement (3-7 wt%; Figure 4C). The most common accessory minerals are ilmenite and diopside. Rare apatite, and zircon occur within submillimetric rodingitic veinlets.

Mineral chemistry of the PTEs-bearing minerals

The PTEs considered in this work are mainly hosted in serpentine minerals (Cr, Ni, and Co), spinel-group minerals (Cr, Ni, and Co), pyroxenes (mainly Cr and subordinately V and Ni), olivines (mainly Ni), chlorites (Cr and Ni), tremolite (V, Co, and Ni), talc (Ni and Cr), ilmenite (V), and weathering products (mainly Fe-oxides and -oxyhydroxides which are strongly enriched in Ni, Cr, and subordinately Co) (Figure 5). Representative chemical analyses of the main minerals are reported in Table S1 in Supplementary Materials.

Serpentine minerals

Serpentine minerals (antigorite and subordinately chrysotile) are the main mineral species in the three rock groups (PSP, MS, and FS) and in all textural (i.e., pseudomorphic and non-pseudomorphic textures) and structural domains (i.e., veins and fractures). The main PTEs hosted in serpentine minerals are Cr and Ni, and subordinately Co, Zn, V, and Cu (Figure 5). Among the serpentine minerals, antigorite is the main PTEs-bearing mineral showing the highest concentration and the widest ranges of Cr (101-9397 ppm), Ni (244-3131 ppm), Zn (10-1113 ppm), Co (13-673 ppm), and V (3-415 ppm). The wide variations in Cr and Ni evidence significant correlation with the different serpentinite groups or textural/structural domain both for antigorite and chrysotile (Figure 6). Antigorite occurring in mesh textures after olivine is invariably enriched in Ni (up to 3198 ppm) with respect to that occurring in bastites (up to 1283 ppm), which on the contrary evidence the highest Cr content (up to 9397 ppm) and not-negligible amount of other PTEs (Co, V, Zn, and Cu). Antigorite occurring in non-pseudomorphic textures (interlocking and interpenetrating) or in evolved and deformed pseudomorphic textures (such as ribbon texture) show the highest compositional variation both for Cr and Ni.

In contrast, chrysotile in veins and in pseudomorphic textures is characterized by relatively low and quite homogeneous Cr and Ni contents (Figure 6).

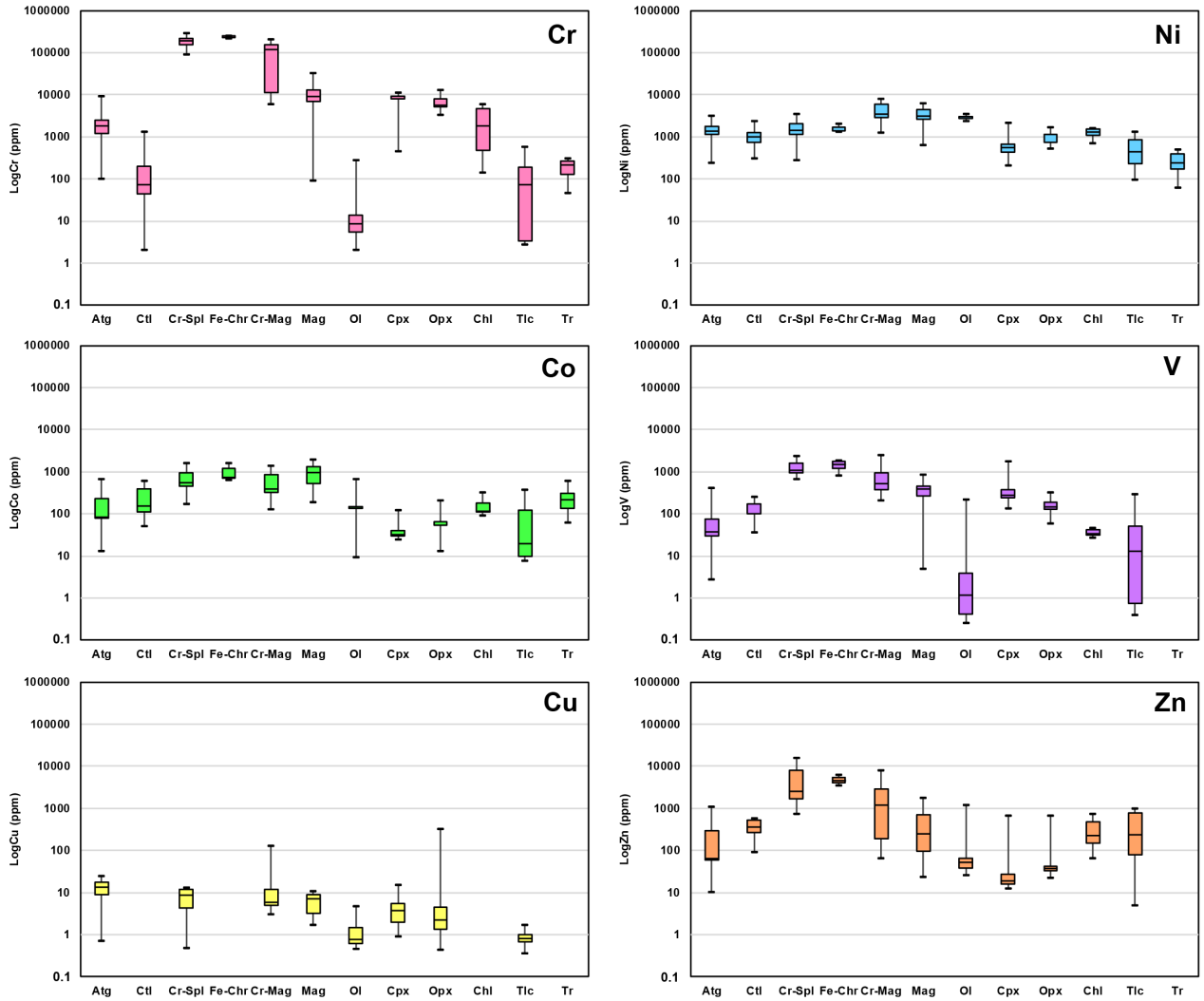

Figure 5. Box plots showing statistical parameters of concentrations (in ppm) of Cr, Ni, Co, V, Cu, and Zn in the different minerals. Vertical lines show the range in concentrations, the boxes are bounded by the 1st and 3rd quartile values, and the horizontal line inside the box represents the median value. Mineral abbreviations after Whitney and Evans (2010).

Spinel-group minerals

Spinel-group minerals occur in all the rock groups and have a wide compositional range covering the fields of Cr-spinel (in PSP), ferrian chromite, Cr-magnetite (both in PSP and in MS), and magnetite (in all three rock groups; Figure 7). These crystallochemical variations appear to be strictly related to the degree of serpentinization. The main PTEs hosted in spinel-group minerals are Cr, Zn, and Ni, and subordinately Co, V, and Cu (Figure 5). As a general rule, other than Cr, V and Zn content decreases from Cr-spinel (median Cr 202660 ppm, V 1132 ppm, Zn 2680 ppm) toward magnetite (median Cr 9201, Zn 258 ppm, V 407 ppm); conversely, Ni and Co increase from Cr-spinels (median Ni 1480 ppm and Co 579 ppm) to magnetite (median Ni 3133 ppm and Co 1032 ppm). In general, Cu is present in a negligible amount in all spinel-group minerals (up to 131 ppm).

Olivines and pyroxenes

Olivines contain a high concentration of Ni (2326-3514 ppm; median 2921 ppm) and non-negligible amounts of Co (9-661 ppm; median 141 ppm) (Figure 5).

Among the silicates, enstatite is the main Cr-bearing phase (3344-13000 ppm; median 5830 ppm); clinopyroxenes (augites and diopside) have the highest concentration and the widest ranges of Ni (207-2200 ppm; median 580 ppm) and V (135-1793 ppm; median 300 ppm). Zn, Cu, and Co are always present in a negligible amount (Figure 5).

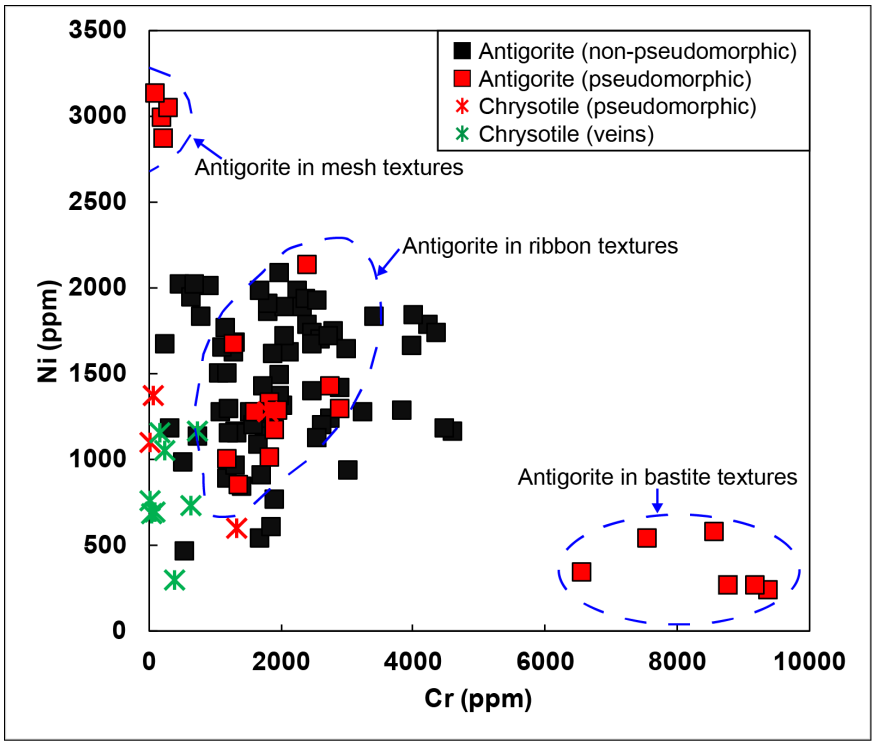

Figure 6. Cr vs Ni contents (ppm) of antigorite and chrysotile in the studied rocks grouped according to the micro-structural or -textural features.

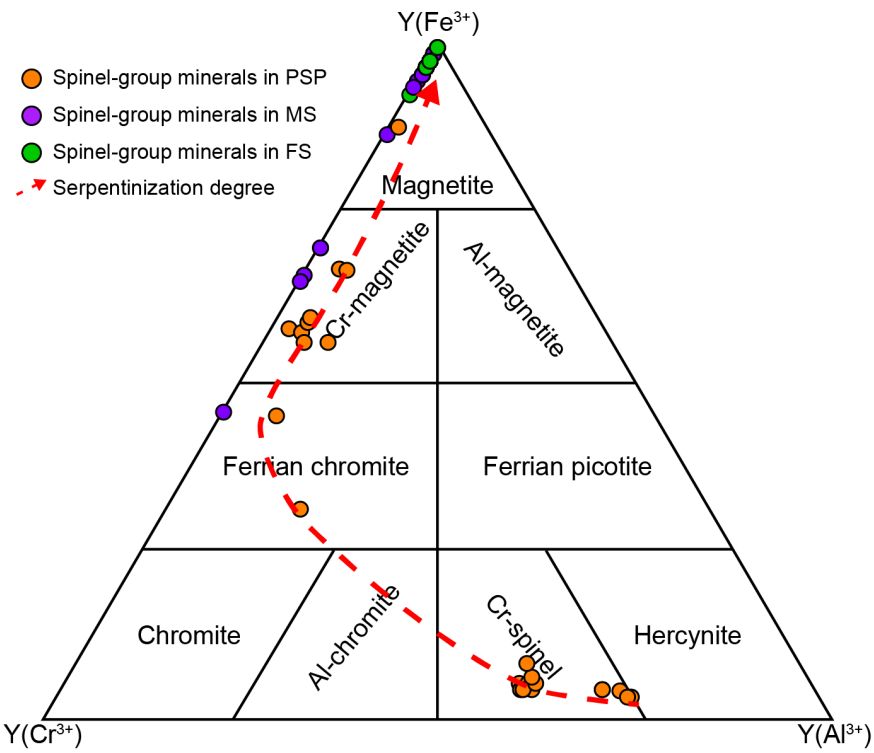

Figure 7. Spinel-group minerals classification diagram (Al^{3+}, Cr^{3+}, and Fe^{3+}); compositional fields are from Stevens, 1944; Haggerty, 1991; Zussman et al., 1992; Gargiulo et al., 2013).

Chlorites, tremolite, and talc

Chlorites (mainly clinochlore) occur in PSP as coronas around Cr-spinel porphyroclasts whereas they form cryptocrystalline to microcrystalline aggregates intimately associated with antigorite in pseudomorphic and non-pseudomorphic textures or with chrysotile in several vein types. Clinochlore in PSP is an important career of PTEs (Figure 5), showing high contents and a wide range of Cr (141-5916 ppm), Ni (717-1626 ppm), and subordinately Zn (66-731ppm) and Co (90-326 ppm).

Talc mainly occurs as vein filling associated with magnetite and chrysotile in the three rock groups. Talc shows a wide range of Ni (97-1334 ppm) and Zn (5-1005 ppm), and subordinately of Cr (3-580 ppm) and Co (8-377 ppm; Figure 5).

Tremolite is mainly concentrated in the salband of MS and FS developing close to tremolite-chlorite hybrid rocks. Tremolite is generally characterized by significant and quite homogeneous concentrations of Cr, Co, and Ni (up to 312, 617, and 512 ppm, respectively) (Figure 5).

Accessory phases

Ilmenite is a widespread accessory mineral in FS where it occurs associated with magnetite both in trails developed along the main foliation and in aggregates. Other than Ti, ilmenite is an important career of V (up to 20391 ppm) and Zn (up to 1880).

Authigenic minerals

The main authigenic phases forming by oxidation and weathering of primary minerals are Fe-oxides (hematite) and -oxyhydroxides (goethite) which occur as partial to complete replacement after magnetite or form cryptocrystalline aggregates within veins or in the surrounding oxidation halos. Although the chemical analyses of these minerals systematically refer to the bulk chemistry of the aggregates, the PTEs concentration of Fe-oxides and oxyhydroxides is generally very high (Ni up to 51000 ppm, Cr up to 8370 ppm, Co up to 1924 ppm, and V up to 376 ppm).

Bulk chemistry

The three groups of ultramafic rocks under investigation are characterized by significant variations of Mg, Si, and, subordinately, Fe. The MgO/SiO_2 ratio falls in the range of subduction-related serpentinites (1.3-0.7; Deschamps et al., 2013) and systematically decreases with the increasing serpentinization degree (from about 1 in PSP to about 0.7 in MS and FS).

Although also the other major elements define quite large compositional range (Al_2O_3=0.9-3.52 wt%; FeO_{tot}= 4.2-11.49 wt%; CaO=0.05-2.67 wt%; TiO_2=0.02-1.30 wt%; MnO_{tot}=0.06-0.2 wt%), these variations are not related to the degree of serpentinization. The only exception is represented by FeO_{tot}, which reaches the highest concentration in the MS (which have the highest content of magnetite and oxidation products) and by TiO_2 which systematically reaches the highest concentration in FS and MS associated with tremolite-chlorite hybrid rocks.

Among the minor and trace elements, Cr, Co, and Ni, and subordinately Cu, V, and Zn are systematically present in significant concentrations (Figure 9 and Table 2).

Cr and Ni have always the highest concentrations and widest range of variability. Cr and Ni vary systematically with the rock types (i.e., with the degree of serpentinization) and show opposite trends with negative and positive correlations with MgO, respectively (Figures 9A-B). Cr reaches the highest concentration (4183 ppm) in MS and decreases to 884 ppm with increasing MgO content in PSP (Table 2 and Figure 9A). On the other hand, Ni has the highest concentration in PSP (3900 ppm) and lowest in MS (1051 ppm; Table 2 and Figure 9B). Co content is very homogeneous in PSP whereas shows a wider variation range in FS and, particularly, in MS where it reaches the highest concentrations (334 ppm; Figure 9C). Cu, with a variation range between 2 to 75 ppm, has a similar behaviour to Co (Figure 9D).

The other PTEs (i.e., Zn and V) do not show clear correlations to the degree of serpentinization, although there are sometimes significant differences in the three different groups considered. V content is very similar in the three rock groups (varying from 13 to 58 ppm) with the lowest concentrations occurring systematically in FS, whereas zinc content appears to be randomly distributed, although in a narrow range of variation (30-63 ppm) (Figures 9E-F).

DISCUSSION

Our results evidence that Cr, Ni, and, subordinately, Co are invariably the PTEs with the highest concentrations; in addition, V, Cu, and Zn are generally found in high concentrations. These results fall in the compositional fields obtained from several authors both in the studied area (Cortesogno et al., 1979; Ernst and Piccardo, 1979; Bonifacio et al., 1997; Rampone et al., 2005; Rampone and Borghini, 2008) and in other ultramafic complexes worldwide (Deschamps et al., 2013 and reference therein) (Figure 8).

The mobility of elements during serpentinization has been discussed for a long time (Deschamps et al., 2013 and references therein), and the debate is still open.

Generally, the process of serpentinization is considered essentially isochemical for Si, Mg, and Fe (Iyer et al., 2008; Debret et al., 2013 a,b) whereas other elements (i.e., Ca, Al, Cr, and REE) are released to the circulating fluids (Janecky and Seyfried, 1986; Douville et al., 2002;

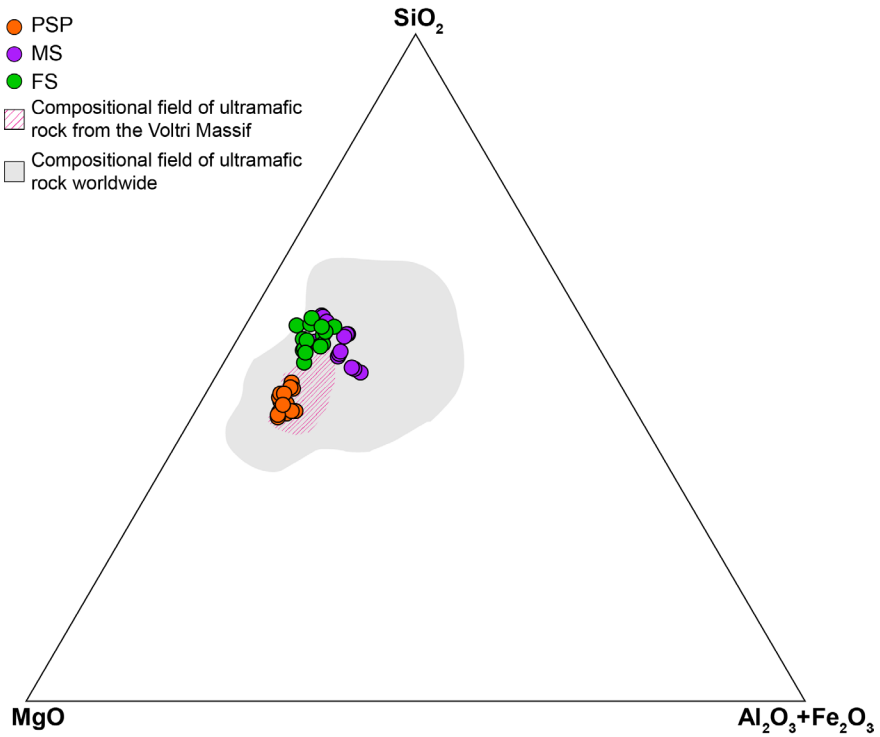

Figure 8. Compositional variations of ultramafic rocks for SiO_2, MgO, Al_2O_3+FeO. Pink dashed areas refer to the composition of the Erro-Tobbio peridotites (Rampone et al., 2005); gray fields refer to the composition of ultramafic rocks worldwide (Angelone et al., 1993; Oze et al., 2004 a,b; Quantin et al., 2008; Caillaud et al., 2009; Kodolànyi et al., 2011; Barnes et al., 2013; Deschamps et al., 2013 and reference therein; Kierczak et al., 2016).

Table 2. Main descriptive statistic parameters (average - Avg, median - M, minimum - Min, maximum - Max, and standard deviation - SD values) for major, minor element, and selected PTEs in the bulk rock (ICP-AES and XRF data), based on fifteen samples for each rock group. Major and minor elements are reported as oxide wt%; selected PTEs are reported in ppm.

Rock	PSP					MS					FS				
	Avg	M	Min	Max	SD	Avg	M	Min	Max	SD	Avg	M	Min	Max	SD
MgO	39.55	39.90	36.01	42.60	1.95	27.94	28.25	26.60	28.88	0.81	31.34	31.06	28.30	35.75	2.33
Al_2O_3	1.67	1.58	1.01	3.52	0.54	1.66	1.64	0.90	2.51	0.60	1.38	1.40	1.01	1.60	0.17
SiO_2	39.94	40.05	38.42	41.09	0.79	44.87	43.66	41.22	49.30	2.86	47.33	46.80	45.84	49.01	1.06
CaO	1.80	2.00	1.02	2.67	0.48	0.35	0.15	0.12	1.24	0.41	0.47	0.38	0.05	1.26	0.42
TiO_2	0.07	0.07	0.07	0.08	0.01	0.08	0.08	0.04	0.10	0.02	0.04	0.03	0.02	0.07	0.02
MnO_t	0.09	0.09	0.08	0.09	0.00	0.14	0.15	0.06	0.20	0.05	0.12	0.13	0.07	0.15	0.03
Fe_2O_{3t}	7.99	8.06	6.60	9.75	0.96	9.33	10.31	5.53	12.77	2.33	7.00	7.21	4.67	8.57	1.16
V	39	36	27	96	17	50	52	33	58	8	26	31	13	48	13
Cr	1327	1257	884	2700	425	2899	2603	1473	4183	1038	2057	2106	1305	3020	397
Co	84	81	73	103	9	211	212	74	334	74	107	105	57	190	44
Ni	2767	2700	1663	3900	811	1902	2057	1051	2212	430	1350	1370	1093	1730	183
Cu	13	11	2	27	7	27	22	11	58	15	24	13	7	75	21
Zn	45	44	33	60	9	46	44	38	63	8	40	37	30	54	9

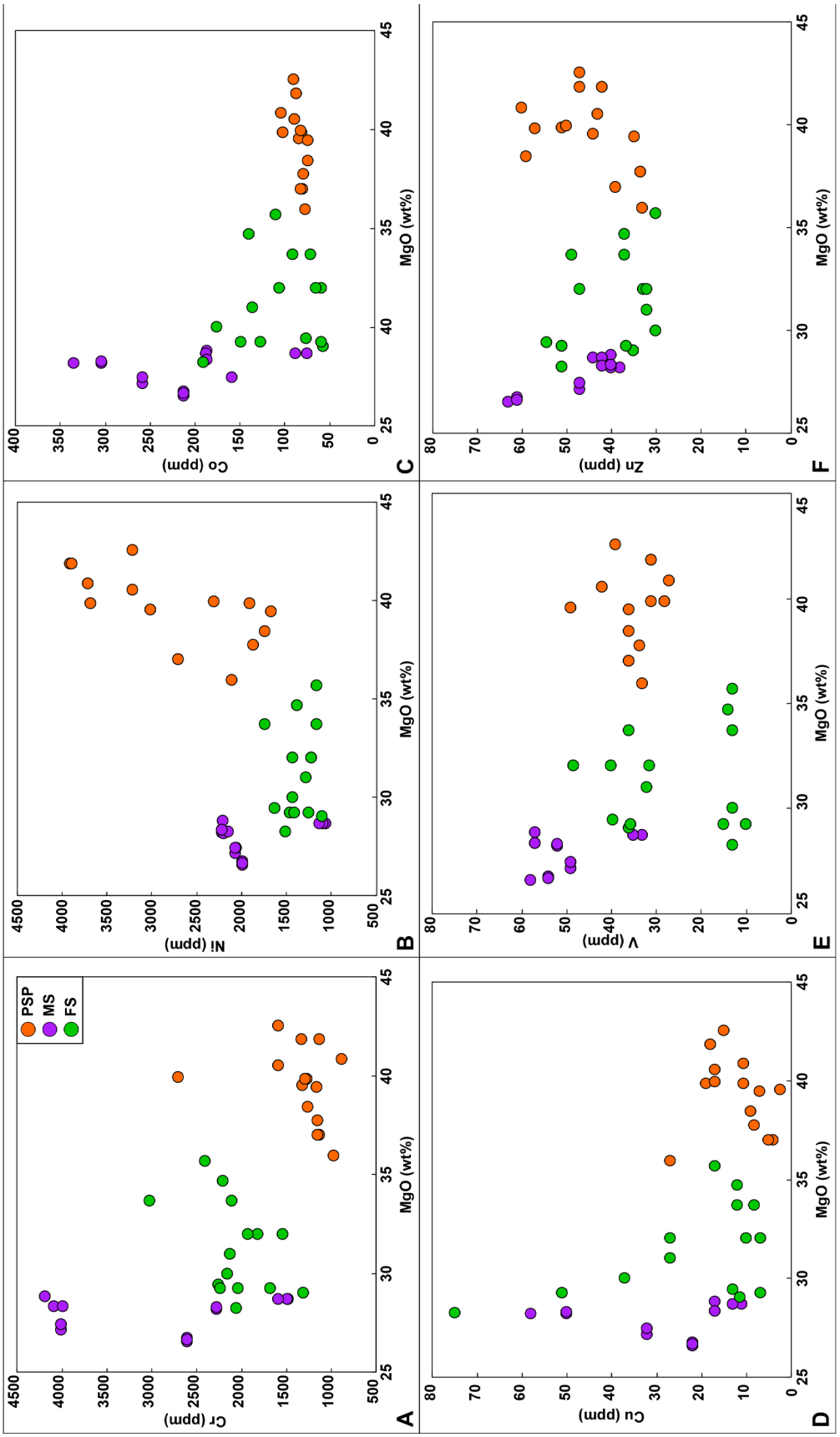

Figure 9. Dispersion plots showing the relationships between A) MgO vs Cr, B) MgO vs, Ni, C) MgO vs Co, D) MgO vs Cu, E) MgO vs V, and F) MgO vs Zn.

Shervais et al., 2005; Paulick et al., 2006; Augustin et al., 2012; Barnes et al., 2013). Concerning Ni and Co, Gulaçar and Delaloye (1976) suggest an isochemical behaviour on a kilometre scale, with relative remobilization of these elements on a smaller scale (centimetric to metric). On the other side, other authors mention that the process of serpentinization has no evident effect on the abundances of Ni, and Co (as well as Cr) in ultramafic rocks (Stueber and Goles, 1967; Govindaraju, 1994; Aziz et al., 2011).

Our results highlight that Cr and, subordinately Co tend to significantly increase with the serpentinization degree in good agreement with several works (e.g., Gahlan and Arai, 2006; Li and Lee, 2006; Paulick et al., 2006) whereas Ni decrease from PSP toward MS and FS (Figures 8 and 9). The main factors controlling the PTEs distribution within the studied ultramafic rocks result the serpentinization degree and the deformation style and intensity which, in turn, strictly control the mineral assemblages and the physico-chemical properties as outlined by various authors (e.g., Gulaçar and Delaloye, 1975; Shervais et al., 2005).

In fact, although Cr-spinel, Al-chromite, and ferrian-chromite are rarely preserved during the increasing serpentinization (i.e., from PSP to MS; Figure 7), the significant chromium enrichment observed in MS can be explained by the progressive increase in Cr-bearing magnetite, which can represent up to 10% of the rock-forming minerals. These minerals tend to pseudomorphically replace primary spinels as well as to crystallize along rims of the mesh-textures, along cleavage planes of bastites, and within veins.

In the FS, the style and intensity of deformation appear to be the main controlling factor in the distribution and concentration of the new-forming Cr-bearing magnetites. In fact, in FS, most of these minerals, which represent up to 5% of the rock-forming minerals, tend to concentrate in millimetric layers or trails parallel to the main foliation. Both in MS and FS the Cr contents of magnetite are generally high (more than 10000 ppm on average) reaching the highest concentrations in pseudomorphs after spinel porphyroclasts (up to 32600 ppm) in MS.

Other than spinel-group minerals, non-negligible amounts of Cr are incorporated in clinochlore (mean value=2550 ppm; Figure 5) and in antigorite, both in non-pseudomorphic (mean value=1960 ppm; Figure 6) and pseudomorphic textures of MS (reaching the highest values, up to 9397 ppm, in bastites, Figure 6; as also observed by Debret et al., 2013a in the Lanzo Massif and Roumèjon et al., 2015 in the Southwest Indian Ridge).

In contrast, the highest concentration and the widest range of Ni are found in the less serpentinized rocks. This behaviour is in good agreement with the results of Li and Lee (2006) from the Feather River Ophiolites (Sierra Nevada Metamorphic Belt, California), but in contrast with those of Gahlan and Arai (2006) from Bou-Azzer ophiolites (Anti-Atlas, Morocco) and Aziz et al. (2011) in the northwestern Zagros Suture Zone (Kurdistan Region, Iraq). The decrease of the Ni concentrations from PSP to FS can be explained with the progressive serpentinization of olivine (the main Ni-bearing minerals in PSP). In fact, only the antigorite after olivine within mesh texture in MS have significant Ni content (up to 3131 ppm) whereas antigorite and chrysotile occurring in other textures and structures within MS and FS contain, on average, 1400 ppm of Ni. The lowest concentrations of Ni are recorded in chrysotile within veins (<302 ppm) and antigorite within bastites (< 500 ppm).

Similar to the Cr behaviour, Co significantly increases from PSP to FS to MS (from 84 to 107 to 221 ppm, respectively) since the main minerals hosting high Co amounts are magnetite and antigorite, occurring within pseudomorphic textures (up to 1879 ppm and 602 ppm, respectively).

The concentrations of V, Zn, and Cu remain almost unchanged during serpentinization without a clear correlation to the degree of serpentinization or the style and intensity of deformation. In fact, Zn and V released from olivine and spinel-group minerals are taken up by antigorite, chlorite, and talc or by accessory phases (e.g., V in ilmenites).

The anomalous high bulk concentration of copper in some MS and FS samples (Figure 9) is presumably due to the occurrence of sulfides (locally observed as micrometric inclusions within Fe-oxides) as also observed by Alt et al. (2012) and Malatesta et al. (2017) in other serpentinites of the Voltri Massif.

Other than primary minerals, a significant contribution to the PTEs content can be provided by authigenic minerals formed in the early stages of rock weathering in supergene conditions. Although our study was not focused to the crystal chemistry of these minerals, the bulk composition of cryptocrystalline to amorphous Fe-oxides (hematite) and -oxyhydroxides (goethite) reveales their affinity to scavenge various metals (particularly Ni, Cr, Co, and V) from the weathering fluids as confirmed in many investigations elsewhere (e.g., Schwertmann and Taylor, 1989; Manceau et al., 2000; Quantin et al., 2002; Becquer et al., 2003; Fandeur et al., 2009; Marescotti et al., 2010; Ho et al., 2013).

CONCLUSION

The knowledge on concentration and behaviour of trace metals in ultramafic rocks is of great interest for their petrological, geochemical, and geodynamic significance. Nevertheless, they have also significant environmental implications since some of these metals are potentially

toxic elements which can be released to soil and water during weathering processes. Although the chemical and mineralogical variation due to serpentinization is well known and debated, few studies are focused on the distribution and variation of elements of environmental concerns due to the mineralogical, textural, and micro-structural feature of similar ultramafic rocks (e.g., Kierczak et al., 2016).

The results of this study, combining the bulk chemistry of outcropping rocks with their geological, structural, mineralogical, and crystallochemical data, may be a useful tool in environmental applications focused in determining the PTEs distribution and in evaluating their mobility and their potential bioavailability as well as in discriminating the natural geochemical background from possible source of contamination.

The general picture of PTEs distribution resulted from this work evidence that only Cr and Ni systematically exceed (up to one order of magnitude) the residential and industrial threshold values according to Italian law (Figure 10; D.M. 471/1999; D.Lgs 152/2006). Among the other elements, only Co evidence concentration of environmental concern, since they are always above the residential threshold values in the three rock groups and above the industrial threshold value in MS.

The multidisciplinary approach used in this work allow to evidence that the most important factors controlling the PTEs variability are the degree of serpentinization (from partially serpentinized peridotites to highly deformed and foliated serpentinites) as well as the style and intensity of deformation, which in turn controls the mineralogical assemblage.

Our study highlighted that spinel-group minerals are by far the main potential source of the PTEs. Nevertheless, several PTEs-bearing phases are also present within either the other rock-forming minerals (i.e., serpentines, olivines, pyroxenes, and chlorites) or various accessory phases (e.g., ilmenite and other oxides, sulphides).

The set of acquired data, appropriately stored in a GIS (Geographic Information System) environment could become a very effective tool for the direct verification of the "geological compatibility" of the PTEs detected in a site with respect to the geological conditions characterizing the territorial context of belonging.

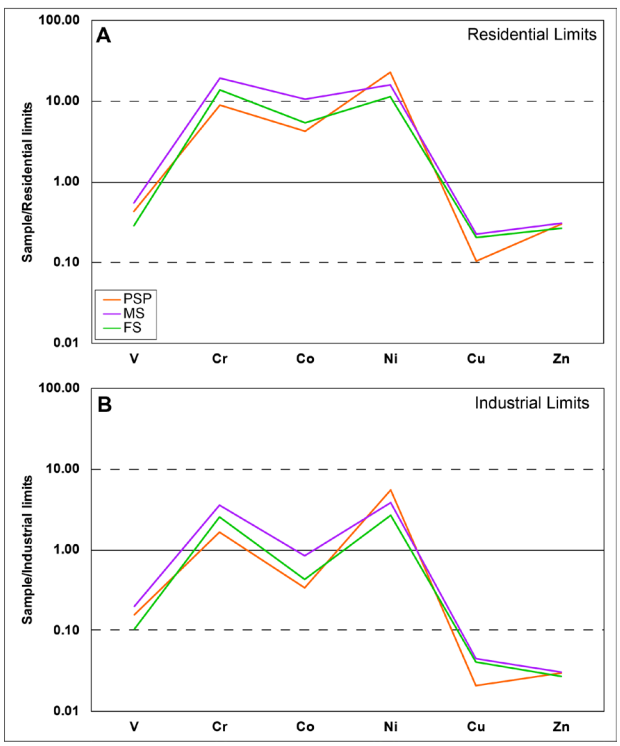

Figure 10. PTEs concentration normalized to Italian threshold values for residential (A) and industrial (B) sites according to Italian law (D.M. 471/1999; D.Lgs 152/2006).

ACKNOWLEDGEMENTS

We thank Dott. Marco Scarsi for critical reading and comments that greatly improved the manuscript. Thanks are also due to the GEOSPECTRA staff for the XRF analyses. The authors wish to thank the reviewers for their insightful and constructive remarks.

REFERENCES

Alexander E.B., 2007. Serpentine geoecology of western North America: geology, soils, and vegetation. Oxford University Press, New York.

Alt J.C., Shanks III W.C., Crispini L., Gaggero L., Schwarzenbach E.M., Früh-Green G.L., Bernasconi S.M., 2012. Uptake of carbon and sulfur during seafloor serpentinization and the effects of subduction metamorphism in Ligurian peridotites. Chemical Geology 322, 268-277.

Angelon, M., Vaselli O., Bini C., Coradossi N., 1993. Pedogeochemical evolution and trace elements availability to plants in ophiolitic soils. Science of the Total Environment 129, 291-309.

Augustin N., Paulick H., Lackschewitz K.S., Eisenhauer A., Garbe-Schönberg D., Kuhn T., Botz R., Schmidt M., 2012. Alteration at the ultramafic-hosted Logatchev hydrothermal field: Constraints from trace element and Sr-O isotope data. Geochemistry, Geophysics, Geosystems 13, 1-20.

Aziz N.R., Aswad K.J., Koyi H.A., 2011. Contrasting settings of serpentinite bodies in the northwestern Zagros Suture Zone, Kurdistan Region, Iraq. Geological Magazine, 148, 819-837.

Barnes J.D., Eldam R., Lee C.T.A., Errico J.C., Loewy S., Cisneros M., 2013. Petrogenesis of serpentinites from the Franciscan Complex, western California, USA. Lithos 178, 143-157.

Becquer T., Quantin C., Sicot M., Boudot J.P., 2003. Chromium

availability in ultramafic soils from New Caledonia. Science of the Total Environment 301, 251-261.

Bonifacio E., Zanini E., Boero V., Franchini-Angela M., 1997. Pedogenesis in a soil catena on serpentinite in north-western Italy. Geoderma 75, 33-51.

Bostrom D., 1987. Single-crystal X-ray diffraction studies of synthetic Ni-Mg olivine solid solutions. American Mineralogist, 72, 965-972.

Butt C.R. and Cluzel D., 2013. Nickel laterite ore deposits: weathered serpentinites. Elements 9, 123-128.

Bystrom A., 1943. Rontgenuntersuchung des Systems MgO-Al_2O_3-SiO_2, Berichte der Deutschen Keramischen Gesellschaft 24, 2-15.

Caillaud J., Proust D., Philippe S., Fontaine C., Fialin M., 2009. Trace metals distribution from a serpentinite weathering at the scales of the weathering profile and its related weathering microsystems and clay minerals. Geoderma, 149, 199-208.

Capitani G.C. and Mellini M., 2006. The crystal structure of a second antigorite polysome (m=16), by single-crystal synchrotron diffraction. American Mineralogist, 91, 394-399.

Capponi G. and Crispini L., 2002. Structural and metamorphic signature of alpine tectonics in the Voltri Massif (Ligurian Alps, North-Western Italy). Eclogae Geologicae Helvetiae 95, 31-42.

Capponi G. and Crispini L., 2008. Note Illustrative della Carta Geologica d'Italia alla scala 1: 50.000 Foglio 213 Genova. SELCA, Firenze.

Capponi G., Crispini L., Federico L., Malatesta C., 2016. Geology of the Eastern Ligurian Alps: a review of the tectonic units. Italian Journal of Geosciences 135, 157-169.

Cheng C.H., Jien S.H., Iizuka Y., Tsai H., Chang Y.H., Hseu Z.Y., 2011. Pedogenic chromium and nickel partitioning in serpentine soils along a toposequence. Soil Science Society of America Journal 75, 659-668.

Cortesogno L., Mazzucotelli A., Vannucci R., 1979. Alcuni esempi di pedogenesi su rocce ultrafemiche in clima mediterraneo. Ofioliti 4, 295-312.

Debret B., Andreani M., Godard M., Nicollet C., Schwartz S., Lafay R., 2013a. Trace element behavior during serpentinization/de-serpentinization of an eclogitized oceanic lithosphere: A LA-ICPMS study of the Lanzo ultramafic massif (Western Alps). Chemical Geology 357, 117-133.

Debret B., Nicollet C., Andreani M., Schwartz S., Godard M., 2013b. Three steps of serpentinization in an eclogitized oceanic serpentinization front (Lanzo Massif-Western Alps). Journal of Metamorphic Geology 31, 165-186.

D.Lgs 152/2006 - Decreto Legislativo n. 152 del 3 aprile, 2006. Norme in materia ambientale. Gazzetta Ufficiale Supplemento ordinario no. 96.

D.M. 471/1999 - Decreto Ministeriale no. 471 del 25 ottobre, 1999. Regolamento recante criteri, procedure e modalità per la messa in sicurezza, la bonifica e il ripristino ambientale dei siti inquinati ai sensi dell'art. 17 del D.Lgs. 22/97 e successive modificazioni e integrazioni. Gazzetta Ufficiale no. 293 del 15 dicembre 1999 Supplemento ordinario 218/L.

Deschamps F., Godard M., Guillot S., Hattori K., 2013. Geochemistry of subduction zone serpentinites: A review. Lithos 178, 96-127.

Douville E., Charlou J.L., Oelkers E.H., Bienvenu P., Colon C.J., Donval J.P., Appriou P., 2002. The rainbow vent fluids (36° 14′ N, MAR): the influence of ultramafic rocks and phase separation on trace metal content in Mid-Atlantic Ridge hydrothermal fluids. Chemical Geology 184, 37-48.

Echevarria G., 2018. Genesis and behaviour of ultramafic soils and consequences for nickel biogeochemistry. In Agromining: Farming for Metals (pp. 135-156). Springer, Cham.

Ernst W.G. and Piccardo G.B., 1979. Petrogenesis of some Ligurian peridotites - I. Mineral and bulk-rock chemistry. Geochimica et Cosmochimica Acta 43, 219-237.

Falini G., Foresti E., Gazzano M., Gualtieri A.F., Leoni M., Lesci I.G., Roveri N., 2004. Tubular-Shaped Stoichiometric Chrysotile Nanocrystals. Chemistry - A European Journal 10, 3043-3049.

Fandeur D., Juillot F., Morin G., Olivi L., Cognigni A., Ambrosi J.P., Guyot F., Fritsch E., 2009. Synchrotron-based speciation of chromium in an Oxisol from New Caledonia: Importance of secondary Fe-oxyhydroxides. American Mineralogist 94, 710-719.

Federico, L., Crispini, L., Scambelluri, M., Capponi, G., 2007. Different PT paths recorded in a tectonic mélange (Voltri Massif, NW Italy): implications for the exhumation of HP rocks. Geodinamica Acta 20, 3-19.

Federico L., Crispini L., Malatesta C., Torchio S., Capponi G., 2015. Geology of the Pontinvrea area (Ligurian Alps, Italy): structural setting of the contact between Montenotte and Voltri Units. Journal of Maps 11, 101-113.

Frondini F., Zucchini A., Comodi P., 2014. Water-rock interactions and trace elements distribution in dolomite aquifers: The Sassolungo and Sella systems (Northern Italy). Geochemical Journal 48, 231-246.

Gahlan H.A. and Arai S., 2006. Genesis of peculiarly zoned Co, Zn and Mn-rich chromian spinel in serpentinite of Bou-Azzer ophiolite, Anti-Atlas, Morocco. Journal of Mineralogical and Petrological Sciences, 0612070013-0612070013.

Gargiulo M.F., Bjerg E.A., Mogessie A., 2013. Spinel group minerals in metamorphosed ultramafic rocks from Río de Las Tunas belt, Central Andes, Argentina. Geologica Acta: An International Earth Science Journal 11, 133-148.

Garnier J., Quantin C., Guimarães E., Garg V.K., Martins E.S., Becquer T., 2009.Understanding the genesis of ultramafic soils and catena dynamics in Niquelândia, Brazil. Geoderma 151, 204-214.

Govindaraju K., 1994. Compilation of working values and sample description for 383 geostandards. Geostandards newsletter 18, 1-158.

Gualtieri A.F., 2000. Accuracy of XRPD QPA using the combined

Rietveld–RIR method. Journal of Applied Crystallography, 33, 267-278.

Gulaçar O.F. and Delaloye M., 1976. Geochemistry of nickel, cobalt and copper in alpine-type ultramafic rocks. Chemical Geology 17, 269-280.

Haggerty S.E., 1991. Oxide textures: a mini-atlas. Reviews in Mineralogy and Geochemistry 25, 129-219.

Hawthorne F.C. and Grundy H.D., 1976. The crystal chemistry of the amphiboles; IV, X-ray and neutron refinements of the crystal structure of tremolite. The Canadian Mineralogist 14, 334-345.

Ho C.P., Hseu Z.Y., Iizuka Y., Jien S.H., 2013. Chromium speciation associated with iron and manganese oxides in serpentine mine tailings. Environmental Engineering Science 30, 241-247.

Hoogerduijn Strating, E.H., 1991. The evolution of the Piemonte-Ligurian ocean: a structural study of ophiolite complexes in Liguria (NW Italy) (Doctoral dissertation, Instituut voor Aardwetenschappen der Rijksuniversiteit Utrecht).

Iyer K., Jamtveit B., Mathiesen J., Malthe-Sørenssen A., and Feder J., 2008. Reaction-assisted hierarchical fracturing during serpentinization. Earth and Planetary Science Letters 267, 503-516.

Janecky D.R. and Seyfried Jr W.E., 1986. Hydrothermal serpentinization of peridotite within the oceanic crust: Experimental investigations of mineralogy and major element chemistry. Geochimica et Cosmochimica Acta 50, 1357-1378.

Kierczak J., Neel C., Bril H., Puziewicz J., 2007. Effect of mineralogy and pedoclimatic variations on Ni and Cr distribution in serpentine soils under temperate climate. Geoderma 142, 165-177.

Kierczak J., Pędziwiatr A., Waroszewski J., Modelska M., 2016. Mobility of Ni, Cr and Co in serpentine soils derived on various ultrabasic bedrocks under temperate climate. Geoderma 268, 78-91.

Kodolányi J., Pettke T., Spandler C., Kamber B.S., Gméling K., 2011. Geochemistry of ocean floor and fore-arc serpentinites: constraints on the ultramafic input to subduction zones. Journal of Petrology 53, 235-270.

Kumarathilaka P., Dissanayake C., Vithanage M., 2014. Geochemistry of serpentinite soils: A brief overview. Journal of Geological Society of Sri Lanka 16, 53-63.

Larson A.C. and Von Dreele R.B., 2004. General Structure Analysis System (GSAS). Los Alamos National Laboratory Report LAUR 86-748.

Li Z.X.A. and Lee C.T.A., 2006. Geochemical investigation of serpentinized oceanic lithospheric mantle in the Feather River Ophiolite, California: implications for the recycling rate of water by subduction. Chemical Geology 235, 161-185.

Malatesta C., Crispini L., Federico L., Capponi G., Scambelluri M., 2012. The exhumation of high-pressure ophiolites (Voltri Massif, Western Alps): Insights from structural and petrologic data on metagabbro bodies. Tectonophysics 568, 102-123.

Malatesta C., Federico L., Crispini L., Capponi G., 2017. Fluid-controlled deformation in blueschist-facies conditions: plastic vs brittle behaviour in a brecciated mylonite (Voltri Massif, Western Alps, Italy). Geological Magazine 155, 335-355.

Manceau A., Schlegel M.L., Musso M., Sole V.A., Gauthier C., Petit P.E., Trolard F., 2000. Crystal chemistry of trace elements in natural and synthetic goethite. Geochimica et Cosmochimica Acta 64, 3643-3661.

Marescotti P., Azzali E., Servida D., Carbone C., Grieco G., De Capitani L., Lucchetti G., 2010. Mineralogical and geochemical spatial analyses of a waste-rock dump at the Libiola Fe–Cu sulphide mine (Eastern Liguria, Italy). Environmental Earth Sciences 61, 187-199.

Messiga B., Piccardo G.B., and Ernst W.G., 1983. High-pressure eo-Alpine parageneses developed in magnesian metagabbros, Gruppo di Voltri, western Liguria, Italy. Contributions to Mineralogy and Petrology 83, 1-15.

Oze C., Fendorf S., Bird D.K., and Coleman R.G., 2004a. Chromium geochemistry in serpentinized ultramafic rocks and serpentine soils from the Franciscan complex of California. American Journal of Science 304, 67-101.

Oze C., Fendorf S., Bird D.K., Coleman R.G., 2004b. Chromium geochemistry of serpentine soils. International Geology Review 46, 97-126.

Paulick H., Bach W., Godard M., De Hoog J.C.M., Suhr G., Harvey J., 2006. Geochemistry of abyssal peridotites (Mid-Atlantic Ridge, 15 20′ N, ODP Leg 209): implications for fluid/rock interaction in slow spreading environments. Chemical Geology 234, 179-210.

Petrelli M., Morgavi D., Vetere F., Perugini D., 2016. Elemental imaging and petro-volcanological applications of an improved laser ablation inductively coupled quadrupole plasma mass spectrometry. Periodico di Mineralogia 85, 25-39.

Quantin C., Becquer T., Berthelin J., 2002. Mn-oxide: a major source of easily mobilisable Co and Ni under reducing conditions in New Caledonia Ferralsols. Comptes Rendus Geoscience 334, 273-278.

Quantin C., Ettler V., Garnier J., Šebek O., 2008. Sources and extractibility of chromium and nickel in soil profiles developed on Czech serpentinites. Comptes Rendus Geoscience 340, 872-882.

Rampone E., Romairone A., Abouchami W., Piccardo G.B., Hofmann A.W., 2005. Chronology, petrology and isotope geochemistry of the Erro-Tobbio peridotites (Ligurian Alps, Italy): records of Late Palaeozoic lithospheric extension. Journal of Petrology 46, 799-827.

Rampone E. and Borghini G., 2008. Melt migration and intrusion in the Erro-Tobbio peridotites (Ligurian Alps, Italy): Insights on magmatic processes in extending lithospheric mantle. European Journal of Mineralogy 20, 573-585.

Rouméjon S., Cannat M., Agrinier P., Godard M., Andreani M., 2015. Serpentinization and fluid pathways in tectonically exhumed peridotites from the Southwest Indian Ridge (62–65

E). Journal of Petrology 56, 703-734.
Savov I.P., Ryan J.G., D'Antonio M., Fryer P., 2007. Shallow slab fluid release across and along the Mariana arc-basin system: Insights from geochemistry of serpentinized peridotites from the Mariana fore arc. Journal of Geophysical Research: Solid Earth, 112(B9).
Scambelluri M., Hoogerduijn Strating E.H., Piccardo G.B., Vissers R.L.M., Rampone E., 1991. Alpine olivine and titanian clinohumite bearing assemblages in the Erro Tobbio peridotite (Voltri Massif, NW Italy). Journal of Metamorphic Geology 9, 79-91.
Scarsi M., Malatesta C., Fornasaro S., 2018. Lawsonite-bearing eclogite from a tectonic mélange in the Ligurian Alps: new constraints for the subduction plate-interface evolution. Geological Magazine 155, 280-297.
Schwertmann U.T.R.M. and Taylor R.M. (1989. Iron oxides. Minerals in soil environments, (mineralsinsoile) 379-438.
Shervais J.W., Kolesar P., Andreasen K., 2005. A field and chemical study of serpentinization-Stonyford, California: chemical flux and mass balance. International Geology Review 47, 1-23.
Spandler, C., Hermann, J., Faure, K., Mavrogenes, J.A., Arculus, R.J., 2008. The importance of talc and chlorite "hybrid" rocks for volatile recycling through subduction zones; evidence from the high-pressure subduction mélange of New Caledonia. Contributions to Mineralogy and Petrology 155, 181-198.
Stevens R.E., 1944. Composition of some chromites of the western hemisphere. American Mineralogist: Journal of Earth and Planetary Materials 29, 1-34.
Stueber A.M. and Goles G.G., 1967. Abundances of Na, Mn, Cr, Sc and Co in ultramafic rocks. Geochimica et Cosmochimica Acta 31, 75-93.
Tashakor M., Yaacob W.Z.W., Mohamad H., Ghani A.A., 2014. Geochemical characteristics of serpentinite soils from Malaysia. Malaysian Journal of Soil Science 18, 35-49.
Whitney D.L. and Evans B.W., 2010. Abbreviations for names of rock-forming minerals. American mineralogist 95, 185-187.
Wright J.P., Bell A.M., Attfield J.P., 2000. Variable temperature powder neutron diffraction study of the Verwey transition in magnetite Fe_3O_4. Solid State Sciences 2, 747-753.
Zanazzi P.F., Montagnoli M., Nazzareni S., and Comodi P., 2006. Structural effects of pressure on triclinic chlorite: A single-crystal study. American Mineralogist 91, 1871-1878.
Zussman J., Howie R.A., Deer W.A., 1992. An introduction to the rock forming minerals. Longman Group Ltd, New York, p 698.